


 Cite this: *Chem. Commun.*, 2026, 62, 4838

 Received 10th November 2025,  
Accepted 3rd February 2026

DOI: 10.1039/d5cc06378g

rsc.li/chemcomm

## Ancestral sequence reconstruction reveals new functional fluorinases and mechanistic insights into enzymatic fluorination

 Shreyas Supekar,<sup>†\*a</sup> Wan Lin Yeo,<sup>†b</sup> Elaine Tiong,<sup>†c</sup> Juliana Rizal,<sup>†d</sup> Ee Lui Ang,<sup>†\*be</sup> Fong Tian Wong,<sup>†\*cd</sup> Yee Hwee Lim,<sup>†\*ce</sup> and Hao Fan,<sup>†\*aef</sup>

**Fluorinases catalyze carbon–fluorine bond formation and represent a rare but valuable enzyme class. We employed ancestral sequence reconstruction to expand fluorinase diversity, identifying seven functional enzymes (28–79% conversion). Comparative analysis revealed previously uncharacterized residues crucial for fluorination, enabling activity rescue in a low-activity ancestral variant.**

The carbon–fluorine bond is widely used in pharmaceuticals, agrochemicals, and materials due to its unique properties, including enhanced metabolic stability and membrane permeability.<sup>1–3</sup> Although fluorine is plentiful in nature, enzymes that incorporate fluorine into organic molecules are extremely rare, with only a few fluorinases identified so far.<sup>4–8</sup> Fluorinase catalyzes nucleophilic S<sub>N</sub>2 substitution of *S*-adenosyl-*L*-methionine (SAM) with inorganic fluoride (F<sup>−</sup>) to produce 5′-fluoro-5′-deoxyadenosine (5′-FDA) and *L*-methionine.<sup>9</sup> Fluorinase functions as a trimer with the active site at the interface of monomers (Fig. 1).<sup>10</sup> Although fluorinases and chlorinases catalyze halide incorporation *via* similar mechanisms, their substrate specificities are notably asymmetric. Fluorinase from *Streptomyces* sp. MA37 (FLA\_MA37),<sup>5</sup> the most efficient

fluorinase characterized to date, can also catalyze chlorination; however, naturally occurring chlorinases cannot perform fluorination.

Given the scarcity of natural fluorinases and their industrial relevance, there is significant interest in expanding their repertoire through protein engineering approaches.<sup>11</sup> Traditional methods like directed evolution and rational design have yielded incremental improvements but are constrained by limited sequence space.<sup>12,13</sup>

Ancestral sequence reconstruction (ASR) enables exploration of deep evolutionary sequence space to access functional proteins beyond the reach of traditional engineering.<sup>14–18</sup> In this study, we apply ASR to fluorinases to expand the biocatalytic toolkit for fluorination. Here, we identified seven catalytically active ancestral fluorinases, with the best ancestral variant matching the activity of top-performing natural fluorinase FLA\_MA37, while exhibiting improved F<sup>−</sup>/Cl<sup>−</sup> selectivity. Comparative sequence analysis revealed key residues for fluorination, validated through targeted mutations that rescued activity

<sup>a</sup> Bioinformatics Institute (BII), Agency for Science, Technology and Research (A\*STAR), 30 Biopolis Street, #07-01 Matrix Building, Singapore 138671, Republic of Singapore. E-mail: supekars@a-star.edu.sg

<sup>b</sup> Singapore Institute of Food and Biotechnology Innovation (SIFBI), Agency for Science, Technology and Research (A\*STAR), 31 Biopolis Way, #04-01 Nanos, Singapore 138669, Republic of Singapore. E-mail: ang\_ee\_lui@a-star.edu.sg

<sup>c</sup> Institute of Sustainability for Chemicals, Energy and Environment (ISCE2), Agency for Science, Technology and Research (A\*STAR), 8 Biomedical Grove, #07-01 Neuros Building, Singapore 138665, Republic of Singapore.

E-mail: wong\_fong\_tian@a-star.edu.sg, lim\_yee\_hwee@a-star.edu.sg

<sup>d</sup> Institute of Molecular and Cell Biology (IMCB), Agency for Science, Technology and Research (A\*STAR), 61 Biopolis Drive, Proteos #07-06, Singapore, 138673, Republic of Singapore

<sup>e</sup> Synthetic Biology Translational Research Program, Yong Loo Lin School of Medicine, National University of Singapore, 10 Medical Drive, Singapore 117597, Republic of Singapore

<sup>f</sup> Institute for Molecular and Cellular Therapeutics, Chinese Institutes for Medical Research, Beijing 100069, China. E-mail: fanhao@cimrbj.ac.cn

† Equal contributions.

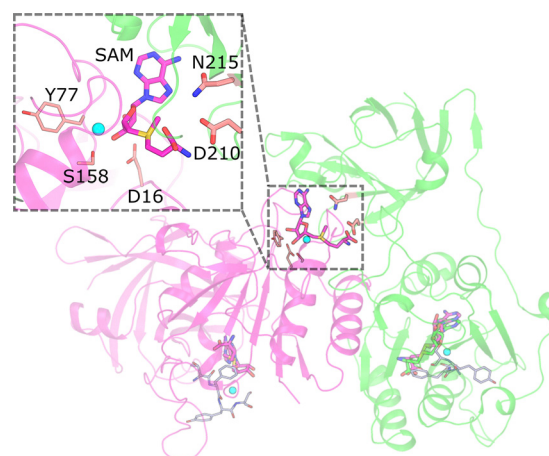


Fig. 1 Fluorinase structure with active-site SAM and F<sup>−</sup> (cyan). Inset: Active site detail.

in a low-performing ancestor, achieving *ca.* 2.2-fold improvement. MD simulations were also employed to identify structural determinants for fluorinase function. These findings demonstrate that ASR effectively expands accessible sequence space beyond traditional enzyme engineering approaches, providing novel biocatalysts and mechanistic insights into these rare enzymes.

To identify candidate sequences for ancestral reconstruction, we started with the fluorinase from *Streptomyces* sp. MA37 (FLA\_MA37, Uniprot: Q70GK9, PDB: 5B6I).<sup>5</sup> The query FLA\_MA37 sequence was searched against NCBI NR database using PSI-BLAST to identify fluorinase homologues. Homologues were filtered for 30–90% sequence identity, appropriate length, and presence of catalytic residues (D16, Y77, S158, D210, N215; Fig. 1), then clustered at 90% identity yielding thirteen representative sequences for ASR. The candidate set comprised thirteen selected homologs including more recently discovered fluorinases from *S. xinghaiensis*, *S. sp.* MA37, *Actinoplanes* sp. N902-109 and *Methanosaeta* sp. PtaU1 (Table S1).<sup>7,19,20</sup> The candidate set also contained a chlorinase from *S. tropica* (SaL)<sup>13</sup> which exhibits distant homology to fluorinases but lacks any fluorination function. The sequences shared 58–94% identity at the amino acid level. Multiple sequence alignment (MSA) of the candidate set was performed with MAFFT.<sup>21</sup> FastTREE<sup>22</sup> was used to construct an initial a maximum likelihood phylogenetic tree for the candidate set MSA (Fig. S1).

The twelve ancestral nodes (ancestral<sub>14</sub> through ancestral<sub>25</sub>) from the phylogenetic tree representing the divergence points in fluorinase evolution were inferred using iqtree<sup>23</sup> suite (Fig. 2). High reconstruction confidence was confirmed with >90% of positions showing posterior probabilities >0.8 (Table S2; SI data). Ancestors shared 38–94% identity with extant homologs (Fig. S2 and Table S3). Reconstructed ancestral<sub>20</sub> was excluded from our ancestral set as it shares 99% sequence similarity with ancestral<sub>19</sub>, yielding eleven putative fluorinases for characterization.

Based our previous work on naturally occurring fluorinases,<sup>5</sup> we optimized solubility conditions to ensure successful expression and characterization. We expressed and tested the activity of two distinct ancestral sequences, specifically ancestral<sub>25</sub>

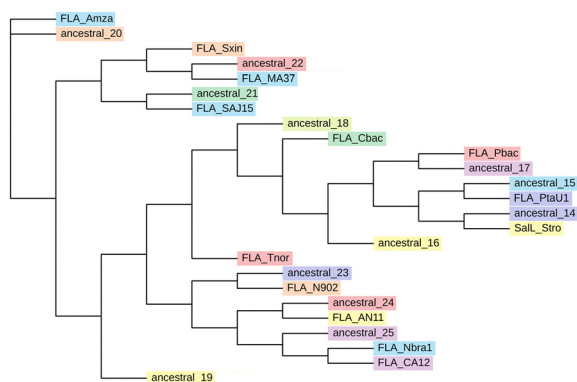


Fig. 2 Phylogenetic tree of candidate set and their respective ancestral fluorinases.

Table 1 NT11-tagged ancestral fluorinases vs. FLA\_MA37. Fluorination and chlorination conversions determined *via* triplicate assays of purified proteins. A\_X indicates ancestral\_X variants. See Table S6 for details

Variant	% conversion (24h)		F/Cl 24h selectivity	Protein melting temperature ( $T_m$ )
	Fluorination	Chlorination		
FLA_MA37	82.20 ± 0.30	15.21 ± 0.16	5.40	48.5 ± 0.1
A_16	28.57 ± 0.03	3.67 ± 0.01	7.79	64.8 ± 0.1
A_19	41.34 ± 0.63	11.37 ± 0.05	3.64	55.8 ± 0.0
A_21	51.76 ± 0.74	19.01 ± 0.10	2.72	50.5 ± 0.4
A_22	79.17 ± 0.87	12.49 ± 0.25	6.34	46.2 ± 0.2
A_23	66.07 ± 0.15	14.68 ± 0.18	4.50	53.2 ± 0.0
A_24	66.88 ± 0.19	15.16 ± 0.19	4.41	54.5 ± 0.1
A_25	52.49 ± 0.17	8.44 ± 0.08	6.22	59.2 ± 0.2
A_16_M13	51.14 ± 0.61	9.25 ± 0.09	5.53	62.0 ± 0.1

and ancestral<sub>15</sub>, using various solubility tags (Table S4). NT11<sup>24</sup> and SUMO<sup>25</sup> solubility tags were chosen were for the expression of the remaining nine ancestral sequences (Table S5).

Fluorination activity (monitoring 5'-FDA formation) of the ancestral enzymes were evaluated using high-throughput (HTP) lysates with SAM and F<sup>-</sup> as substrates. Nine reconstructed enzymes (ancestral<sub>16</sub>-25) demonstrated fluorination activity, while ancestral<sub>14</sub> and ancestral<sub>15</sub> showed no detectable product formation (Table S5). Chloride (Cl<sup>-</sup>) was also tested to check for substrate promiscuity. All active variants retained F<sup>-</sup> selectivity over Cl<sup>-</sup> (Table S5).

To quantify the catalytic performance, we purified the top active variants and determined conversion yields by HPLC (Table 1; see SI methods). We find that all the seven tested fluorinases retained their preference for F<sup>-</sup> over Cl<sup>-</sup>. The best performing ancestral variant, ancestral<sub>22</sub>, exhibited a fluorination capacity comparable to the best known fluorinase FLA\_MA37 (Table 1), while showing higher F<sup>-</sup>/Cl<sup>-</sup> selectivity. To our knowledge, this is the first demonstration that non-natural fluorinases, including ancestral<sub>16</sub>, ancestral<sub>22</sub>, and ancestral<sub>25</sub>, can achieve performance comparable to natural enzymes, with improvement in selectivity. Protein thermal shift assays revealed that most ancestral variants exhibit comparable or better thermostability compared to FLA\_MA37 ( $T_m$  = 48.5 °C), with ancestral<sub>16</sub> showing the highest stability ( $T_m$  = 64.8 °C). Notably, the best-performing variant ancestral<sub>22</sub> exhibits slightly reduced thermostability ( $T_m$  = 46.2 °C), suggesting a potential trade-off between catalytic efficiency and protein stability. Equally important, the addition of these seven new fluorinases to the previous narrow set of 20 known fluorinases expands the available fluorinase repertoire, enabling the identification of new sites for improving enzymatic fluorination.

To identify sequence–function relationships, we examined across four key components of fluorinase: (1) the ion binding site (IBS), (2) the SAM-binding site (SBS), (3) the ion egress site (IES), and (4) the SAM capping loop (SCL) (Fig. 3).

In the IBS, we find that residues T155 and S158 (residue numbering is based on 1RQP) are conserved in all reconstructed sequences (Fig. 3). Ancestral<sub>14</sub> and ancestral<sub>15</sub>, which exhibit no fluorination activity contain the F156W substitution. Interestingly, ancestral<sub>14</sub> and ancestral<sub>15</sub> are the predecessors to SaL\_Stro and FLA\_PtaU1, respectively which

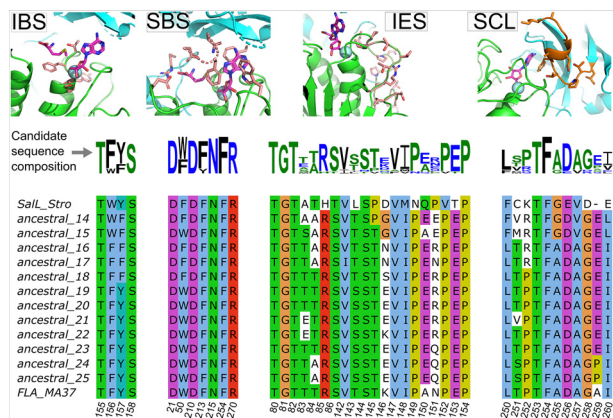


Fig. 3 Sequence variation in key fluorinase catalytic components: ion binding site (IBS), SAM binding site (SBS), ion egress site (IES) and SAM capping loop (SCL). Top: Structure of the sites. Middle: Sequence composition of the candidate set. Bottom: Ancestral sequences vs. FLA\_MA37 and SaLL\_Stro.

also exhibit no activity in our fluorination assays. Substitution Y157F found in ancestral<sub>14–18</sub> also leads to weak or no activity. These sequence-activity correlations suggest that F156W substitution is detrimental to fluorination, while Y157F reduces fluorination efficiency.

For the SBS residues, all positions except W50 are conserved. W50F (Fig. 3, 1RQP numbering) substitution was similarly present in the dead ancestral<sub>14</sub> variant, or the low activity ancestral<sub>16–18</sub> variants, mirroring a similar effect as seen in Y157F in the IBS, indicating W50 might be of functional importance for fluorination. In the IES, a recently identified chain of residues proposed to function as a channel for guiding F<sup>-</sup> to the active site, most residues are conserved. As described previously,<sup>7</sup> T80 and T82, that are crucial to fluorination function are conserved in all predicted ancestors. Similarly, another crucial residue R85, proposed to be the “hook” that guides F<sup>-</sup> ion to the IBS is also conserved in all ancestral sequences. Some variation is seen at T83, N151 and K146 (Fig. 3, 1RQP numbering), especially for moderate to good variants ancestral<sub>19–25</sub>. A lysine residue at position 146, present in FLA\_MA37 and ancestral<sub>22</sub> seems to improve fluorinase function, while K146G substitution, present in ancestral<sub>14</sub> and ancestral<sub>15</sub> leads to abolishment of fluorination function.

The SCL is a 11-residue loop in proximity of the cofactor SAM, that could serve as a gating element that opens to allow SAM access to the fluorinase active site. The role of SCL has not been probed in fluorinase studies yet. In the SCL, while most residues are conserved, we find the substitution A259P (1RQP numbering) in ancestral<sub>24</sub> and ancestral<sub>25</sub> that is not present in other predicted ancestors. Notably, other known fluorinases possess E259 at this position, while the best-performing natural fluorinase, FLA\_MA37, uniquely contains A259. At the position 250, SaLL\_Stro, ancestral<sub>14</sub> and ancestral<sub>15</sub> (no fluorination activity) contain F, while L250 is conserved in all other ancestral sequences and all known fluorinases with fluorination activity. Another interesting variation is seen at the position 252 (Fig. 3, 1RQP numbering), where the chlorinase SaLL\_Stro exhibits a

lysine residue and the low activity ancestral<sub>14–17</sub> contain an arginine residue in this position. Conversely, the better performing ancestral sequences and FLA\_MA37 contain a proline residue in this position. We thus hypothesize that L250 and P252 are important for fluorination, and mutations at position 250 and 252 might lead to abolishment or severe reduction of fluorination activity, respectively.

To investigate whether the identified key residues from sequence–function analysis play a critical role in fluorination activity, we probed ancestral<sub>16</sub>, that exhibits low fluorination activity and contains substitutions at positions 50 (SBS), 157 (IBS), and 252 (SCL). With the goal of enhancing its fluorination capability, we introduced three single mutations into ancestral<sub>16</sub>, namely: F50W (M1), F157Y (M2), and R252P (M3), along with corresponding double mutants M12, M13, M23, and the triple mutant M123. Our high-throughput assays showed that these mutations did not enhance chlorination, which remains undetectable in these enzymes (Table S7). The M1 mutant showed only a slight improvement, while M2 and M3 exhibited no fluorination activity. In contrast, while the mutants M12, M23, and M123 maintained their activity, the mutant M13 (F50W, R252P) mutant exhibited a vast increase in fluorination activity compared to ancestral<sub>16</sub> (~4.3-fold). Upon validation using purified proteins, the M13 mutant showed at least 1.8-fold improvement in fluorination. (Table 1).

To elucidate the mechanistic principles underlying the fluorination capabilities of the predicted ancestral fluorinases, we performed comparative molecular dynamics (MD) simulations of FLA\_MA37, ancestral<sub>22</sub>, ancestral<sub>16</sub>, and the single, double, and triple mutants of ancestral<sub>16</sub> (M1, M2, M3, M12, M13, M23, M123). Homology models were built with Schrodinger<sup>26</sup> using *Streptomyces cattleya* fluorinase (PDB ID: 1RQP) as template. Following equilibration, triplicate all-atom MD simulations (3 × 300 ns) were performed for each system using Desmond.<sup>27</sup> Analysis was performed with MDAnalysis.<sup>28</sup>

The high solvation energy of the fluoride ion renders it a weak nucleophile in the presence of water, potentially hindering its fluorination function. To examine this effect, we calculated water permeation in the vicinity of S158 (SBS) from MD simulations. FLA\_MA37 exhibits the least permeation, followed by ancestral<sub>22</sub> and M13, while ancestral<sub>16</sub>, M23 and M123 show the highest water occupancy (Table 2). Remarkably, this with the experimental observations of fluorination (Table 1 and S5, S7), suggesting that active site hydrophobicity contributes to catalytic efficiency.

The variants ancestral<sub>16</sub>, M2, M3, M12, and M23 show elevated SAM and SBS dynamics, consistent with reduced activity (Fig. S3–S8 and Table S8, see SI for details). To probe mutations at positions 50 (SBS), 157 (IBS), and 252 (SCL), we analyzed key intermolecular distances to SAM or fluoride (Fig. S9). FLA\_MA37 exhibits the most native-like geometry, followed by ancestral<sub>22</sub> and M13. While position 157 shows little conformational variability, position 50 is highly divergent. M1 and M12 fail to form native-like SAM contacts, whereas M13 and M123 restore proper SAM positioning. Position 252 reveals an unexpected mechanism for mutants, where the sidechain of

**Table 2** Water permeation at ion binding site (IBS) (MD simulations). Permeation = water within 3.0 Å of S158 polar hydrogens. Trimer (%): any monomer satisfies the condition. Monomer (%): evaluated for each monomer individually

Variant	Water permeation	
	Trimer (%)	Monomer (%)
FLA_MA37	23.1	7.7
Ancestral_22	42.51	16.14
Ancestral_16	78.93	32.82
Ancestral_16_m1	58.66	28.51
Ancestral_16_m2	64.11	25.93
Ancestral_16_m3	62.78	27.32
Ancestral_16_m12	58.39	27.25
Ancestral_16_m13	45.7	21.88
Ancestral_16_m23	78.07	43.6
Ancestral_16_m123	86.74	44.09

R252 reorients to form a cation- $\pi$  interaction with Y232, destabilizing the  $\beta$ -sheet spanning residues 232–252 and increasing flexibility in the SAM capping loop (Fig. S9–S12).

MD simulations show that single mutants M1, M2, and M3 fail to rescue activity, highlighting the composite nature of the defects. Among double mutants, M13 uniquely restores activity by improving SAM  $\pi$ -stacking while eliminating the disruptive R252–Y232 interaction, yielding native-like SAM positioning and reduced water permeation. Although M123 shows native-like protein and SAM dynamics, it exhibits high water permeation, indicating that active-site dehydration is the dominant determinant of fluorination activity (Fig. S3–S8 and Table 2 and S8).

Despite sequence divergence, fluorination activity is maintained across diverse *Streptomyces* and *Actinoplanes* species. Ancestral\_14 and ancestral\_15 represent evolutionary branches leading to inactivity, suggesting fluorination can be lost through few substitutions (F156W, Y157F, W50F, L250F, R252). The asymmetry between fluorinases (that can chlorinate) and chlorinases (that cannot fluorinate) likely reflects the greater catalytic challenge of fluorination due to fluoride's high solvation energy. Our water permeation analysis confirms that active fluorinases have highly hydrophobic active sites, a requirement for fluorination but not for chlorination. Ancestral\_22 matches FLA\_MA37 activity with marginal improvement in selectivity, suggesting fluorination emerged early and has been evolutionarily conserved.

In summary, fluorination activity persists across diverse ancestral fluorinases but is highly sensitive to substitutions that increase active-site hydration or destabilize SAM binding. Our integrated evolutionary, mutational, and molecular dynamics analyses reveal that strict control of active-site dehydration and SAM positioning are key constraints governing biological C–F bond formation. This work expands the accessible fluorinase sequence space and provides a mechanistic framework for future engineering efforts toward biofluorination.

## Conflicts of interest

There are no conflicts to declare.

## Data availability

The data supporting this article have been included as supporting information (SI) and supporting data. Supplementary information is available. See DOI: <https://doi.org/10.1039/d5cc06378g>.

## Acknowledgements

The authors thank Ravi Kumar Verma for insightful discussions and inputs. The authors acknowledge funding support from Agency for Science, Technology and Research (A\*STAR), Singapore (C211917003, C233017006, and C211917010), and Institute for Molecular and Cellular Therapeutics, Chinese Institutes for Medical Research, Beijing, China.

## References

- 1 M. Inoue, Y. Sumii and N. Shibata, *ACS Omega*, 2020, 5, 10633–10640.
- 2 T. Okazoe, *Proc. Jpn. Acad., Ser. B*, 2009, 85, 276–289.
- 3 J. Wang, M. Sánchez-Roselló, J. L. Aceña, C. del Pozo, A. E. Sorochinsky, S. Fustero, V. A. Soloshonok and H. Liu, *Chem. Rev.*, 2014, 114, 2432–2506.
- 4 C. Dong, F. Huang, H. Deng, C. Schaffrath, J. B. Spencer, D. O'Hagan and J. H. Naismith, *Nature*, 2004, 427, 561–565.
- 5 H. Sun, W. L. Yeo, Y. H. Lim, X. Chew, D. J. Smith, B. Xue, K. P. Chan, R. C. Robinson, E. G. Robins, H. Zhao and E. L. Ang, *Angew. Chem., Int. Ed.*, 2016, 55, 14277–14280.
- 6 X. Feng, Y. Cao, W. Liu and M. Xian, *Front. Bioeng. Biotechnol.*, 2022, 10, DOI: [10.3389/fbioe.2022.881326](https://doi.org/10.3389/fbioe.2022.881326).
- 7 I. Pardo, D. Bednar, P. Calero, D. C. Volke, J. Damborský and P. I. Nikel, *ACS Catal.*, 2022, 12, 6570–6577.
- 8 R. K. Verma, W. L. Yeo, E. Tiong, E. L. Ang, Y. H. Lim, F. T. Wong and H. Fan, *Chem. Sci.*, 2025, 16, 10610–10619.
- 9 C. D. Cadicamo, J. Courtieu, H. Deng, A. Meddour and D. O'Hagan, *ChemBioChem*, 2004, 5, 685–690.
- 10 T. Kittilä, P. Calero, F. Fredslund, P. T. Lowe, D. Tezé, M. Nieto-Domínguez, D. O'Hagan, P. I. Nikel and D. H. Welner, *Microb. Biotechnol.*, 2022, 15, 1622–1632.
- 11 S. Purser, P. R. Moore, S. Swallow and V. Gouverneur, *Chem. Soc. Rev.*, 2008, 37, 320–330.
- 12 H. M. Senn, D. O'Hagan and W. Thiel, *J. Am. Chem. Soc.*, 2005, 127, 13643–13655.
- 13 A. S. Eustáquio, F. Pojer, J. P. Noel and B. S. Moore, *Nat. Chem. Biol.*, 2008, 4, 69–74.
- 14 E. A. Gaucher, S. Govindarajan and O. K. Ganesh, *Nature*, 2008, 451, 704–707.
- 15 M. J. Harms and J. W. Thornton, *Nat. Rev. Genet.*, 2013, 14, 559–571.
- 16 D. L. Trudeau and D. S. Tawfik, *Curr. Opin. Biotechnol.*, 2019, 60, 46–52.
- 17 Y. Gumulya, J.-M. Baek, S.-J. Wun, R. E. S. Thomson, K. L. Harris, D. J. B. Hunter, J. B. Y. H. Behrendorff, J. Kulig, S. Zheng, X. Wu, B. Wu, J. E. Stok, J. J. De Voss, G. Schenk, U. Jurva, S. Andersson, E. M. Isin, M. Bodén, L. Guddat and E. M. J. Gillam, *Nat. Catal.*, 2018, 1, 878–888.
- 18 B. S. Jones, C. M. Ross, G. Foley, N. Pozhydaieva, J. W. Sharratt, N. Kress, L. S. Seibt, R. E. S. Thomson, Y. Gumulya, M. A. Hayes, E. M. J. Gillam and S. L. Flitsch, *Angew. Chem., Int. Ed.*, 2024, 63, e202314869.
- 19 L. Ma, Y. Li, L. Meng, H. Deng, Y. Li, Q. Zhang and A. Diao, *RSC Adv.*, 2016, 6, 27047–27051.
- 20 H. Deng, L. Ma, N. Bandaranayaka, Z. Qin, G. Mann, K. Kyeremeh, Y. Yu, T. Shepherd, J. H. Naismith and D. O'Hagan, *ChemBioChem*, 2014, 15, 364–368.
- 21 K. Katoh and D. M. Standley, *Mol. Biol. Evol.*, 2013, 30, 772–780.
- 22 M. N. Price, P. S. Dehal and A. P. Arkin, *PLoS One*, 2010, 5, e9490.
- 23 L.-T. Nguyen, H. A. Schmidt, A. von Haeseler and B. Q. Minh, *Mol. Biol. Evol.*, 2015, 32, 268–274.
- 24 T. K. M. Nguyen, M. R. Ki, R. G. Son and S. P. Pack, *Appl. Microbiol. Biotechnol.*, 2019, 103, 2205–2216.
- 25 J. G. Marblestone, S. C. Edavettal, Y. Lim, P. Lim, X. Zuo and T. R. Butt, *Protein Sci.*, 2006, 15, 182–189.

- 26 M. P. Jacobson, D. L. Pincus, C. S. Rapp, T. J. F. Day, B. Honig, D. E. Shaw and R. A. Friesner, *Proteins*, 2004, **55**, 351–367.
- 27 K. J. Bowers, D. E. Chow, H. Xu, R. O. Dror, M. P. Eastwood, B. A. Gregersen, J. L. Klepeis, I. Kolossvary, M. A. Moraes, F. D. Sacerdoti, J. K. Salmon, Y. Shan and D. E. Shaw, in SC '06: Proceedings of the 2006 ACM/IEEE Conference on Supercomputing, 2006, pp. 43–43.
- 28 N. Michaud-Agrawal, E. J. Denning, T. B. Woolf and O. Beckstein, *J. Comput. Chem.*, 2011, **32**, 2319–2327.